DOI: 10.1109/TNB.2016.2594483

"Catch the Pendulum": The Problem of Asymmetric Data Delivery in Nanoscale Communication Networks

Nabiul Islam, *Student Member, IEEE*, and Sudip Misra, *Senior Member, IEEE*
Indian Institute of Technology, Kharagpur, Pin: 721302, India
{nabiuli, smisra}@sit.iitkgp.ernet.in

***Abstract*—The network of novel nano-material based nanodevices, known as nanoscale communication networks or nanonetworks, has ushered a new communication paradigm in the Terahertz Band (0.1-10 THz), promising revolutionization of ubiquitous healthcare, e.g., monitoring of chronic cardiovascular diseases unobtrusively. However, the limited communication range up to few centimeter of such nanodevice poses a serious problem on the mechanism of data delivery from the underlying nanoscale communication networks to macro-world networks characterized by radio propagation. In this work, first we envisage a novel architecture for *Coronary Heart Disease* (*CHD*) monitoring system consisting of nanodevice-embedded Drug Eluting Stents (DESs), which are termed as nanoDESs. Next, we study the problem of asymmetric data delivery in such nanonetwork-based systems and propose a simple distance-aware power allocation algorithm, *catch-the-pendulum*, which optimizes the energy consumption of nanoDESs. The algorithm exploits the periodic change in mean distance between a nanoDES, inserted inside affected coronary artery, and the nano-macro interface which is fitted in the intercostal space of the rib cage of a patient suffering from a CHD disease. Extensive simulations confirm superior performance of the proposed algorithm with respect to energy consumption, packet delivery, and shutdown phase.**

***Index Terms*—Nanoscale communication networks, multi-scale communication, asymmetric data delivery, coronary heart disease, ubiquitous healthcare.**

I. Introduction

One of the challenging problems in today's global healthcare is combating against high mortality rate due to CHD [1], [2]. The disease develops because of the narrowing of the inner cavity of a coronary artery, essentially hindering the normal blood supply to heart muscle and ultimately leading to the cause of *myocardial infarction* [2]. The process of constriction involves gradual deposition of fatty materials including *bad* cholesterol on the inner walls of coronary arteries. The diagnosis and treatment of CHD disease involves administering medications, and complex medical surgical procedures including *Percutaneous Transluminal Coronary Angioplasty* (*PTCA*) and *stenting*. *Coronary Artery Bypass Grafts* (*CABG*) are also performed during critical stages of the disease – stable/advanced CHD [3], [4].

The morbidity of recovering from the disease after undergoing surgical procedures is ineffective: statistics claim that CHD requires frequent hospitalization and incurs high medical costs [5], [6]. Furthermore, the adverse effect of revascularization, or Percutaneous Coronary Intervention (PCI) procedures include the recurrence of stenosis, known as restenosis, which causes renarrowing of the arteries. It is reported [7], [8] that multiple revascularizations require even after six months of primary PCI, to break the plaques inside the coronary arteries. If restenosis is not properly detected and corrected, it may trigger to the death of a patient [9], [10]. In addition, highly sophisticated procedures involving the insertion of DES inside the occluded region of the arteries – which ultimately suppress local cell proliferation by releasing drug locally – has been shown to yield improved results than the insertion of Bare Metal Stent (BMS), a metal tube-like structure which is usually inserted into the the site of blockage to widen the lumen of arteries [11]. However, advanced DESs are also often inefficacious to prevent late *thrombosis* because of irregular, disproportionate drug disposal by drug-eluting stents. For example, Venkatraman et al. [12] reported that slow-release *sirolimus* DESs provided more effective than fast-release DESs. However, neither of these prevent late restenotic cell growth effectively. To summarize, studies reported in [12]–[14] suggest that drugs should be administered controllably and adaptively – i.e., the specific amount of dose will be administered based on the temporal and spatial change of unintended cell growth inside the artery. Therefore, optimal release profile of drugs, by taking into all the above-mentioned factors, is a crucial challenge to medical practitioners.

Growing progress of nanotechnology-based nanomaterial has provided us fabrication tools to build nano-scale devices equipped with processing and communication circuits, which can sense and transmit cellular and molecular level parameters, such as glucose and cholesterol [15]. On the other hand, nanoparticle-based drug and gene-eluting stents for combating CHD are in the research pipeline [16]. Meanwhile, information and communication technology (ICT) is increasingly moving toward providing innovative solution in diverse fields such as ubiquitous healthcare service provisioning, including diagnostics and holistic well-being monitoring, with affordable price.

In this paper, we envisage a novel architecture of CHD monitoring system consisting of network of nanodevice-embedded DESs (nanoDESs), which is surgically deployed inside lesions of coronary arteries. A nanodevice is made of nano-scale processing and communication components, such as nano-transistor, nano-battery, and nano-transceiver. The nanoDES controls the release of drugs using interactive commands from healthcare professionals, via the nano-macro (NM) interface which is inserted inside the intercostal space of the rib cage of

a CHD patient. Fig 2 illustrates the architecture of such a CHD monitoring system, which we will describe later elaborately. The limited resources of a nanodevice – particularly, its energy and storage, and distinct properties of the Terahertz band, such as high molecular absorption loss – result in limited communication range and coverage area. Such constraint on communication range poses significant barrier on delivering data from the underlying nanonetworks to macro-scale communication networks, often at least for nanonetworks-based CHD monitoring system, rendering the problem of *asymmetric* data delivery. The asymmetric data delivery problem may appear when a nano-transceiver-enabled nanodevice, due to its limited communication range and energy storage, dispenses significant effort (in the sense that a nanodevice spends considerable amount of energy, relative to its energy content) only in delivering data from the underlying nanoscale communication networks to a device operating in macro-scale communication networks, referring here to the radio communication. On the contrary, the macro-scale device may not experience such burden in delivering data back to nano-scale communication domain since the device is technically assumed to possess relatively large amount of energy.

To optimize energy consumption in asymmetric data delivery settings, we propose a simple distance-aware power allocation algorithm, named as *catch-the-pendulum* (*CAP*), which exploits the periodic change in mean distance between a nanoDES, which is placed inside affected coronary artery, and the nano-macro (NM) interface, which is placed in the intercostal space of the rib cage of a patient suffering from a CHD disease. The main contributions of our work are as follows:

- Proposing a novel nanonetworks-based architecture for CHD monitoring system for ubiquitous healthcare applications
- Studying the problem of asymmetric data delivery in multi-scale communication settings (here, multi-scale refers communication between nanoscale and macro-scale communication paradigm)
- Proposing a novel distance-aware power allocation algorithm for improved network performance.

The rest of the paper is organized as follows. Section II outlines the related works on data delivery and nanonetworks-based healthcare applications. Section III elaborates the motivation and description of asymmetric data delivery in nanonetworks-based CHD system. The system models are described in Section IV, while Section V focuses on the main design of CAP algorithm. The performance of the algorithm is presented in Section VI. We discuss the feasibility study of the proposed nanoDES-based CHD monitoring system and the effects of spatial distribution of NM on the system performance in Section VII. In Section VIII, we summarize and outline the possible extension of the work.

II. Related Works

Existing works on data delivery in nanonetworks-based CHD monitoring can be categorized into two dimensions: (1) architectural design of nanonetworks-based healthcare applications, and (2) communication and networking aspects of those applications. On the research progress of nanonetworks-based healthcare technologies, Malak and Akan [17] discussed relationship among various intra-body molecular communication mechanisms such as neuro-spike communication for nervous system, and action-potential-based communication for cardiac system. They are also introduced different channel models for different communication mechanisms. Guo et al. [18] proposed an in vivo wireless nanosensor network (iWNSN), which can be deployed inside human organs to monitor molecular activities of the organelles in real time. Furthermore, experiments were performed to quantize channel properties of the Terahertz band inside human tissues. The results indicated new research challenges, including the design of novel modulation schemes [19]. As an example of nanonetworks-based ubiquitous healthcare monitoring, Misra et al. [20] envisaged a green wireless body area nanonetwork having both electromagnetic and molecular nanoscale communication modes and harvesting energy from the organ's mechanical and biochemical energy source. Their proposed game-theoretic solutions optimized energy consumption by mutually choosing a targeted communication mode. On the other hand, Stankovic [21] envisaged that the growing progress on Internet of things (IoT) would enable pervasive and personalized healthcare through remote sensing and monitoring of human wellness. In this regard, Internet of Nano Things (IoNT), which augments IoT in the nano dimension, has been proposed [22] to access inside such human organelles which are unreachable by traditional networks. In summary, these works are in the early stages, primarily focusing on defining a robust architecture of the nanonetworks and addressing mechanism of the underling nanodevices, and proposing protocols for medium access and system management. However, to the best of our knowledge our work is the first to address data delivery issues between *the nanoscale and macro-scale communication domains in context of CHD monitoring*.

Considerable amount of works on data delivery or data forwarding schemes were published concerning wireless networks, specifically wireless sensor networks [23]. For example, Couto et al. [24] demonstrated the efficacy of the proposed metric *Expected Transmission Count ETX*), which selected the high throughput paths in forwarding data to destination in multi-hop wireless networks with lossy links. Lu et al. [25] proposed a heuristic method to schedule the sleeping patterns of nodes in duty-cycled WSNs to optimize the delivery latency of the nodes. However, considering both unreliable wireless links and energy-efficient duty-cycled schedule Gu and He [26] proposed *Dynamic Switch based Forwarding* algorithm to optimize the network performance in terms of expected delivery ratio, communication delay, and energy consumption. In addition, Zhao et al. [27] addressed the problem in different settings, which included mobile agents roaming inside the network to collect data, as well as multiple mobile sink nodes in large-scale networks. However, in delay-tolerant networks, the performance of data delivery is often compromised with the cost of message overhead often used for predicting the pattern of mobility of nodes [28].

Our work is distinct from others on several respects: (1) we are the first, to best of our knowledge, to address

the issues of asymmetry in data delivery process emanating from the communication between nanoscale and macro-scale communication networks; (2) we exploit the unique periodic mobilities of both the source and sink nodes to design power saving algorithm; and finally, (3) we envisage the architecture of the CHD monitoring system, which has been motivated by the rapid progress on multiple disciplines including nanotechnology-based drug delivery, novel nanomaterial-based tiny sophisticated devices, and new communication paradigms, such as bio-inspired molecular communication, and nanoscale communication networks.

III. Asymmetric Data Delivery in Nanoscale Communication Netowrks

A. Communication in Terahertz band

The nanodevices, imprinted into the DESs, communicate the luminal profile of coronary arteries to healthcare provider via nano-macro interface in electromagnetic communication mode. The operating frequency of such nano-scale communication lies in the Terahertz band [29]. The band exhibits unique properties such as *molecular absorption loss*, which occurs mainly due to the absorption of wave energy by molecules available in the transmission medium, such as water vapor, nitrogen, and oxygen, which cause significant signal attenuation [30]. Piesiewicz et al. [31] reported that attenuation due to this molecular absorption phenomenon could shoot up to hundreds of dB per km. Moreover, *free space loss* in this band is significantly higher, as evident from Friis free space transmission formula – which essentially says that the path loss is proportional to the square of link distance and frequency components of the transmitting signal. With free space path loss of $102 - -112$ dB at 10 m communication range, total loss (molecular absorption loss plus free space loss) can accrue few hundreds of dB. To compensate such large attenuation factor, high gain directional antenna has been proposed for the indoor high speed personalized devices, providing significant performance up to few meters from the transmitter [32].

B. Motivation for asymmetric data delivery

Jornet and Akyldiz [29] and Yang et al. [33] reported that communication range in the Terahertz band for nanonetworks shrinks to few centimeters due to its ultra-low power budget of a nanodevice. Furthermore, the total path loss changes about tens of dB for the deviation of few mm distance in a centimeter-communication link [30]. Although the use of high gain antenna can compensate such high path loss, for many biomedical applications, enabling such high power antenna violates the biological safety standard specified in IEEE Standard C95.1-2005 [34]. In addition, as the proposed CHD monitoring system is to be deployed in and on the human body, *dielectric constants* of various biological tissues such as blood and muscle having significant amount of conductivity in higher frequency [35] would affect signal strength adversely since signal attenuation has relation with electrical conductivity and dielectric constant [36]. Based on these facts, we summarize that the communication range reduces and varies substantially even with small variation of distance in the order of mm. Such reduced communication range adds significant complexity on data delivering from nanoscale communication networks to the nano-macro interface.

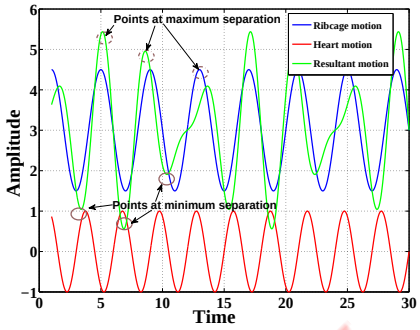

Fig. 1. Minimum and maximum separation points

IV. Preliminaries and System Model

A. System architecture

The network of nanoDESs can provide real-time information about the profile of restenosis around the stents and release anti-restenosis drugs precisely and effectively. Such efficacy on CHD monitoring is possible because of expert decision, which is derived from combing the nanonetworks-acquired rules and control fed by healthcare provider through the nano-macro interface. Fig. 2 depicts architecture of the system, which has two major components:

- *Nanodevice-embedded Drug Eluting Stents* (*nanoDESs*): The nanodevices, which are capable of measuring lumen constriction, communicate such information, and control the release the drugs such as *sirolimus*, or *paclitaxel*, are imprinted onto the stents. The stents are engineered to accommodate nanodevices using NEMS technology. Based on this technology, the actuation components of nanodevices are programmed to open the caps of drug reservoirs and close them smoothly. It is noted that plurality of nanodevices per stents might be realizable, depending on the requirements of applications. The deployment strategy of nanoDESs follows the same technology as adopted by bare DESs – i.e., *catheter* technology.
- *Nano-macro interface* (*NM*): It basically acts as a gateway between the nano-world (metaphorically, referring to the network of underlying nanoscale communication networks) to the macro-world (referring to the Internet). The interface is inserted in the intercostal space of the rib cage of a CHD patient. The interface is placed strategically– either fixed by the proposed networking algorithm or accorded with a clinically suitable position, which is based on the condition of patient and the decision of practitioners. To enable communications in both the scales (nano-macro and vice versa, and macro), the NM interface houses transceiver circuitries for either communication scale technologies – THz and RF (radio frequency).

The nanoDESs are expected to harvest energy from the periodic mechanical movement of heart to replenish its nano-batteries using the component piezoelectric nanogenerators, which consists of ZnO nanowires and leverage the wires' piezoelectric effect caused by repeated compression and elon-

gation. The magnitude of harvested energy depends on the size of the array of nanowires and the capacity of the nano-capacitors. Due to the nanoDES's small size, the device assumes limited harvesting capacity[1]. Accordingly, the nanoDESs follow the energy harvesting mechanism, as described in [37].

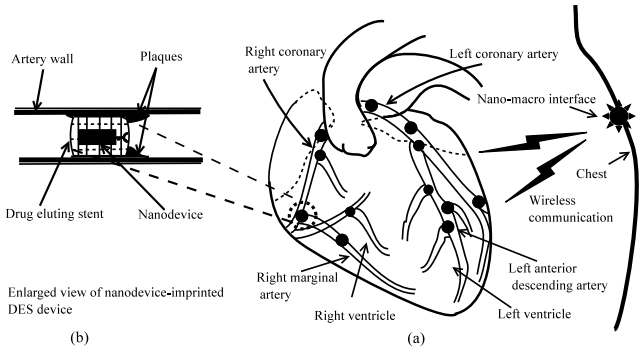

Fig. 2. Proposed network architecture

B. Position and shape of heart

We observe that the individual distances of nanoDESs, placed on either single or multiple coronary arteries with its branches and sub-branches, from the nano-macro interface vary according to their spatial distribution on the heart's surface. Eventually, the spatial distribution of the arteries on the heart dictates the nodes' spatial distribution. Therefore, the study on the model of shape and location of human heart with respect to rib cage is inevitable.

Anatomically, the heart is located in the middle of chest or *thoracic* cavity (known as middle mediastinum). With respect to the rib cage, it is in the posterior of the body of *sternum* and is second to the fifth intercostal space [38], as shown in Fig. 3. The heart's position is slanted in thorax and left of the mid line. Furthermore, the heart's wall is covered with a double membrane sac, known as *Pericardium* consisting of three distinct part: (a) *Epicardium*, known as the surface of the heart; (b) *Myocardium*, the thick cardiac muscles containing blood vessels, receiving nutrients from the coronary arteries which spread out the epicardium; and (c) *Endocardium*, covering the hollow chambers of the heart. The chambers are divided into four components: (1) left atrium and (2) right atrium, and (3) left ventricle and (4) right ventricle. the shape of ventricle can be modeled as ellipsoid, cylindrical or a eggshell [39], [40].

C. Model of the dynamics of the heart

The periodic motion of heart, known as cardiac cycle, is divided mainly into two main phases:

1) Systole (i.e., contraction of ventricles), which refers to the time span during which the right and left ventricles contract and eject blood to pulmonary and aorta arteries, respectively.
2) Diastole (i.e., relaxation of ventricles), which refers to the time span during which de-oxygenated blood from *superior* and *inferior* vena cava returns to right ventricle through the right atrium, and oxygenated blood from pulmonary veins reaches the left ventricle via the left atrium. This blood circulatory system with Wiggers diagram, a chart representing cardiac activity, is illustrated in Fig. 8.

[1]For the sake of brevity of the paper, we skip elaborating it.

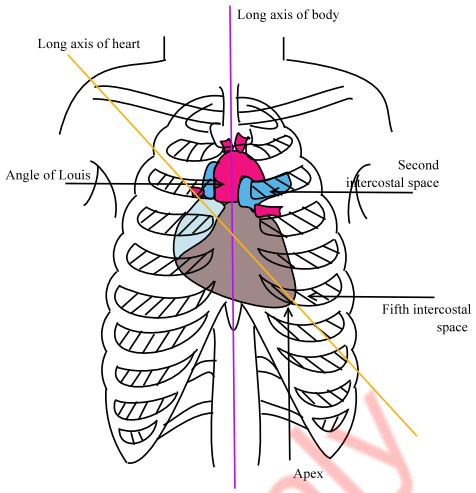

Fig. 3. Anatomical position of heart

Accompanying with every cardiac cycle, the heart muscle undergoes contraction and relaxation, alternately – which, in medical term, are called as strain or deformation. The left ventricle, modeled as a thick-walled cylinder, or in more realistic form, an ellipsoid, [39] experiences three types of deformation: *Longitudinal*, *Circumferential*, and *Transmural* or *wall thickening*.

- *Longitudinal*: This deformation or shortening is observed along the long axis of the heart (see Fig 3) and is mainly due to the displacement of mitral annular plane, called as *Mitral Annular Plane Systolic Excursion* (*MAPSE*).
- *Circumferential*: This refers to the shortening of the mid-wall radius of ventricle. Illustrated in Fig. 7, the radius is shown in a cross-section of an ellipsoid representing the left ventricle.
- *Transmural* or *wall thickening*: It is assumed to occur due to the property of incompressibility exhibited by myocardium, the property through which the volume of the the wall remains constant regardless of contraction or expansion of the heart. As a result, the wall between endocardium and epicardium layers widens when the ventricle contracts.

The value of heart wall deformations varies according to the measurement methodologies and modes, such as M-mode, B-mode, ultrasound imaging, 2D/3D tissue doppler and speckle tracking, and MRI (Magnetic Resonance Imaging) [41]. However, we consider, without loss of generality and heterogeneity, the measurements of those shortening, as given in [39], to compute other parameters, such as periodic deformations with respect to body axes system. We describe such computational steps in the Appendix.

Accorded with the activity of cardiac cycle, the deformation of the ventricle is periodic and can be modeled as a sinusoidal function. The function fits significantly with the real data, as shown in Fig. 5

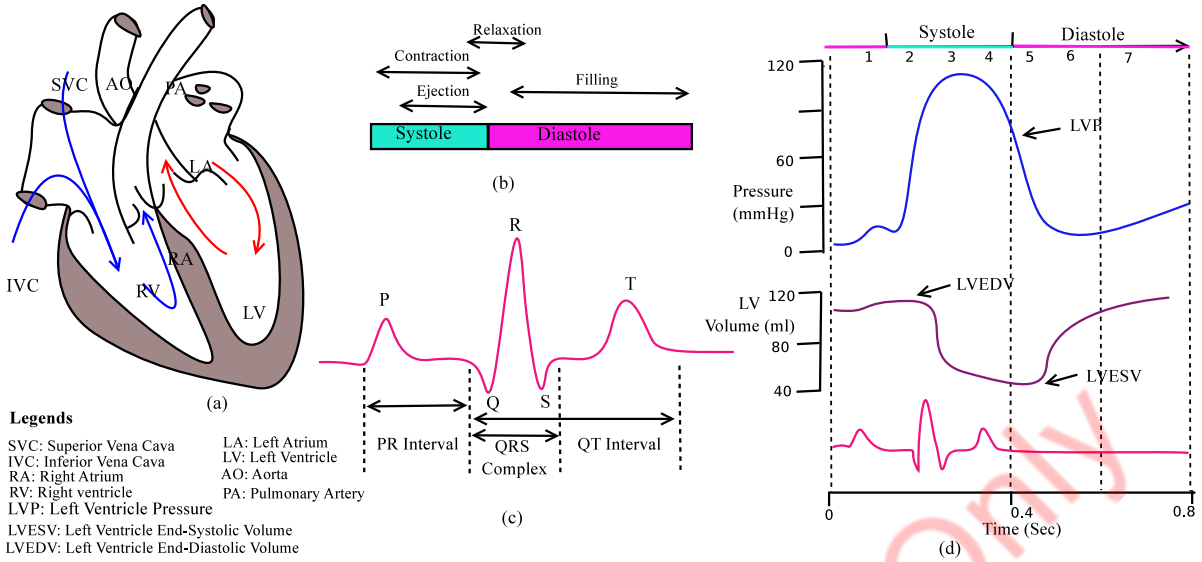

Fig. 4. Relation of heart's periodic motion with pressure and electrical activity

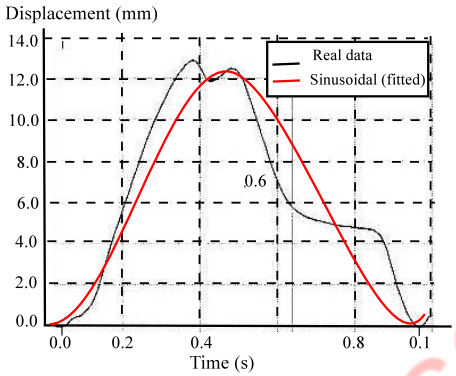

Fig. 5. Curve based on real data (adopted from [40]), and sinusoidal curve (red)

D. Model of the movement of thoracic cage

Due to inspiration and expiration, the thoracic cage, a bony enclosure consisting of ribs and costal cartilages with vertebral column posteriorly and sternum anteriorly, undergoes periodic movement in three major directions or diameters: (1) *Anteroposterior*, or *sagittal* – due to the movement of sternum, the motion resembles the movement of a *pump handle*; (2) *Lateral* or *Transverse* – due to the lateral elevation of ribs that articulate the sternum anteriorly and vertebral column posteriorly, the lateral excursion often corresponds to the movement of a *bucket handle*; and (3) Vertical – due to the contraction and relaxation of diaphragm muscle, the rib cage periodically increases and decreases in vertical direction [42]. In particular, the thoracic cage moves as a result of synchronized and active participation of the lungs, the respiratory muscles, and the diaphragm; the periodic inflow and outflow of air into the alveoli in the lungs create a gradient of pressure, and consequently, the change in volume of thoracic cavity results in such movement.

The magnitude of those thoracic movement was measured with various techniques and apparatuses [42], [43], and the values varied with plurality of parameters, such as ethnicity and race, demography, and individualistic trait. For the sake of simulation and validation of the proposed system, we consider, without loss of generality and heterogeneity, the measurements as reported in [43]. Meanwhile, the periodic motion of thoracic movement can be shown to model as a sinusoidal function, as is the case with heart's periodic motion, which is illustrated in Section IV-C.

E. Location of coronary artery

To assess the risk of developing atherosclerotic plaques and corresponding regional myocardial abnormalities, the American Heart Association (AHA) categorized coronary vessels into three major branches: (1) RCA, Right Coronary Artery; (2) LAD, Left Anterior Descending Coronary Artery; and (3) LCX, Left Circumflex artery [44]. However, such arterial distributions can be observed using different imaging principles and modalities, such as coronary angiography, positron-emission tomography (PET), and cardiomagnetic resonance (CMR), and different angiographic projections, including left and right anterior oblique views (LAO, RAO) with angulations. Without loss of generality and heterogeneity, we consider the work of Dodge et al. [45] on the anatomical locations of various important segments of coronary arteries. In Fig. 6, the segements are shown with respect to three principal body axes system: (a) Lateral, (b) Vertical, and (c) Antiposterior. At this point, we mention that all the measurements, including the location of nano-macro interface and distances between a nanoDES and the nano-macro interface are made, based on this body axes system.

V. Main Design

The nanoDESs of the system, which are deployed on the surface of the human heart (inside the coronary arteries, which extend the surface to heart muscle) are expected to be few centimeters far away, on an average, from the nano-macro interface, placed into the intercostal space. Such assumption on the average distance separations is based on the work [46],

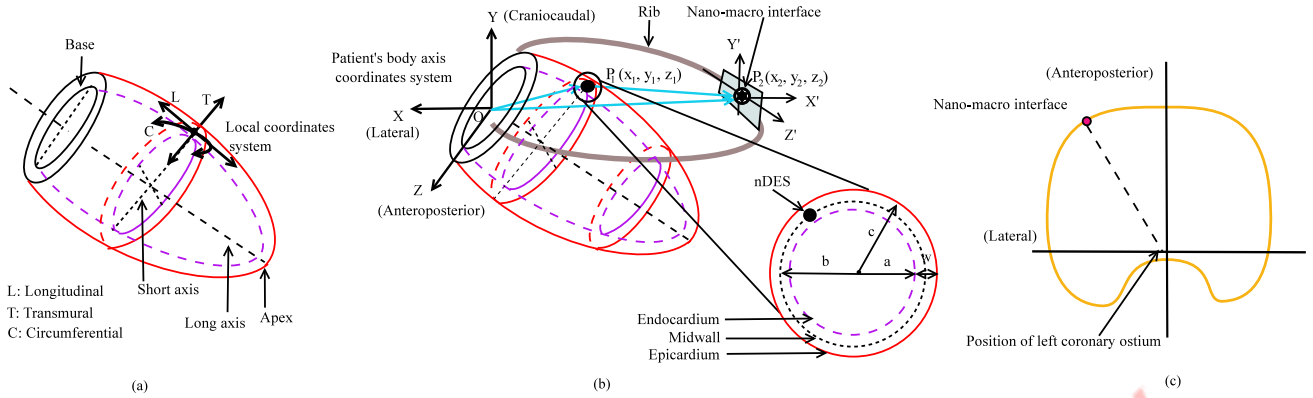

Fig. 7. Some relevant geometric variables of left ventricle modeled as a half ellipsoid (a) and coordinate systems used to compute distance between nanoDES, inserted inside a coronary artery, and nano-macro interface, placed at the ribcage (b). Cross section of a rib cage labelled with the coordinate axes (c).

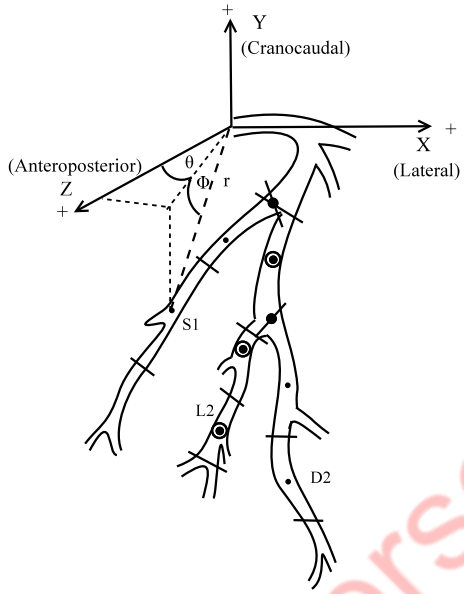

Fig. 6. Major coronary segments and body axes system (adopted from [45]). The origin is chosen at the ostium of left coronary artery and also served same for computing distance between a nanoDES to the nano-macro interface

which shows that the anatomical separation between the apex of heart to nearest intercostal muscle is few centimeters. However, the periodic inflation and contraction of heart muscle due to its *systolic* and *diastolic* pressure, and that of the rib cage due to the breathing process, inhalation and exhalation, causes this separation to prolong and shorten over time. Should the data delivery from the nanonetworks to nano-macro interface be allowed randomly in time, it might so happen that the signal does not reach the nano-macro interface with desirable strength due to the longest distance to cover, which occurs when both the rib cage and heart reach their extreme opposite positions because of their different speeds (or frequencies) of motions. This phenomenon is illustrated in Fig. 8. We exploit such periodic change in distance to design a *distance-aware power allocation algorithm*. The basic idea of this algorithm is to send data when the distance between a nanoDES and the nano-macro interface is minimal. Such minimal points are found to be periodic, as depicted in Fig. 7, for this CHD monitoring system. We leverage these minimal points in time domain as the time instants nanoDESs can transmit data. In later subsection, we describe the theory related to finding minimal points.

A. Computing distance between a nanoDES to the nano-macro interface

The periodic motion of ribcage can be modeled as a sinusoidal function, written as follows:

$$y_r = a_r \sin(2\pi f_r t + \phi_r) \tag{1}$$

where f_r is the frequency, measured per second, and a_r is the amplitude of the motion of rib cage. The constant ϕ_r is termed as the initial phase. The variable r is the instantaneous position vector. Similarly, the motion of the heart can be modeled as

$$y_h = a_h \sin(2\pi f_h t + \phi_h) \tag{2}$$

where f_r is the frequency of the heart per second and a_h is the amplitude of the motion of heart measured from the mean position. Similarly, the constant ϕ_h refers to the initial phase.

To measure the instantaneous distance between a nanoDES and the nano-macro interface, first we choose the body axes system as a three-dimensional coordinate system, with origin at the position of the ostium of the left ventricle. Since estimating the distance of nano-macro interface from the perspective of a nanoDES is of primary concern, we calculate the distance as follows:

$$\begin{aligned} r &= y_r - y_h \\ &= y_r - y_h \\ &= a_r \sin(2\pi f_r t + \phi_r) - a_h \sin(2\pi f_h t + \phi_h) \end{aligned} \tag{3}$$

Theorem 1. *The minimal distance between rib cage and heart is achieved at time* $t = \frac{2}{w_r + w_h} \times \left(2n\pi - \frac{\phi_r + \phi_h}{2}\right)$, *where* w_r *and* w_h *are angular frequencies corresponding to periodic motions of rib cage and heart, respectively, and* $n \in \mathbb{Z}^+$

Proof. We observed that the maximum or minimum distance is achieved when both the pendulums's instantaneous positions are in opposite directions and extreme positions. The pendulums represent the periodic motion of the heart and rib cage,

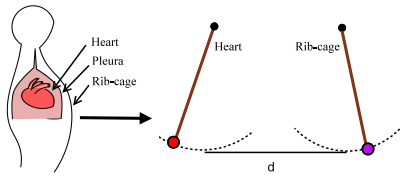

Fig. 8. Modeling the periodic motions of rib cage and heart motion as pendulums

as illustrated in Fig 8. Using the relation $-1 \geqslant \sin\theta \leqslant 1$, we infer

$$\begin{aligned} r_{max} &= d + a_r + a_h \quad \text{and} \\ r_{min} &= d - (a_r + a_h) \end{aligned} \tag{4}$$

where d is the distance between a nanoDES and the nano-macro interface when they are the equilibrium positions (equilibrium, in the context of the motion of pendulums, representing the resting position). It is noted that the heart wall cannot touch the ribcage, which, mathematically, is stated in the following condition:

$$d > a_r + a_h \tag{5}$$

To compute the time instants for the extreme values of r, the quantity $y_r - y_h$ is maximized. Meanwhile, from Equations (1) and (2), the normalized instantaneous distances of the two pendulums is written as follows:

$$\begin{aligned} \frac{y_r}{a_r} &= \sin(2\pi f_r t + \phi_r) = \sin(w_r t + \phi_r) \text{and} \\ \frac{y_h}{a_h} &= \sin(2\pi f_h t + \phi_h) = \sin(w_h t + \phi_h) \end{aligned} \tag{6}$$

Eventually, the problem of maximizing $y_r - y_h$ reduces to the problem of maximizing $\frac{y_r}{a_r} - \frac{y_h}{a_h}$. Hence, we obtain the following expression:

$$\begin{aligned} \frac{y_r}{a_r} - \frac{y_h}{a_h} &= \sin(w_r t + \phi_r) - \sin(w_h t + \phi_h) \\ &= \sin(w_r t + \phi_r) + \sin(\pi + w_h t + \phi_h) \\ = 2\sin(\frac{w_r + w_h}{2} t + \frac{\pi + \phi_r + \phi_h}{2}) &\cos(\frac{w_h - w_r}{2} t + \frac{\phi_h - \phi_r + \pi}{2}) \\ = \underbrace{2\cos(\frac{w_h - w_r}{2} t + \frac{\phi_h - \phi_r + \pi}{2})}\, &\sin(\frac{w_r + w_h}{2} t + \frac{\pi + \phi_r + \phi_h}{2}) \end{aligned} \tag{7}$$

where the underbrace quantity denotes the varying amplitudes of the periodic motion, which is the combination of periodic motions of both the heart and the rib cage. In order to maximize $\frac{y_r}{a_r} - \frac{y_h}{a_h}$, the following condition must be satisfied:

$$\begin{aligned} &\sin(\frac{w_r + w_h}{2} t + \frac{\pi + \phi_r + \phi_h}{2}) = 1 \\ &\therefore \frac{w_r + w_h}{2} t + \frac{\pi + \phi_r + \phi_h}{2} = 2n\pi + \frac{\pi}{2}, \text{where } n \in \mathbb{Z}^+ \\ &\Rightarrow \frac{w_r + w_h}{2} t = 2n\pi + \frac{\pi}{2} - \frac{\pi + \phi_r + \phi_h}{2} \end{aligned} \tag{8}$$

From Equation (8), we obtain the required time instants at the point of minimal distance separations, which are given below:

$$t = \frac{2}{w_r + w_h}\left(2n\pi - \frac{\phi_r + \phi_h}{2}\right) \tag{9}$$

□

Algorithm 1 "Catch-the-pendulum:" Distance-aware power allocation

Inputs: Distance (d), Minimum Signal-to-Noise-Ratio (SNR_{min}) to decode a packet
Output: Transmission power (P_T)

Find L_f and L_a ▷ L_f: free propagation loss ▷ L_a: absorption loss
if $L_f \times L_A < \frac{P_T^c}{P_r^{min}}$ **then** ▷ P_r^{min}: receiver power at SNR_{min} ▷ P_T^c: current transmission power
    $P_T^{min} \leftarrow P_r^{min} \times L_f \times L_A$
    $P_T \leftarrow P_T^{min}$
else
    $\epsilon \leftarrow P_r^{min} - \frac{P_T^c}{L_f \times L_A}$
    $P_T^{min} \leftarrow P_T^c + \epsilon \times L_f \times L_A$
    $P_T \leftarrow P_T^{min}$
end if

Algorithm 2 Naive approach

Inputs: Distance (d), Minimum Signal-to-Noise-Ratio (SNR_{min}) to decode a packet
Output: Transmission power (P_T)

Find L_f and L_a ▷ L_f: free propagation loss ▷ L_a: absorption loss
Calculate current transmission power P_T^c
$P_T^c \leftarrow P_r^{min} \times L_f \times L_A$ ▷ P_r^{min}: receiver power at SNR_{min}
if $P_T^c < P_r^{min}$ **then**
    $\epsilon \leftarrow P_r^{min} - P_T^c$
    $P_T \leftarrow P_T^c + \epsilon \times L_f \times L_a$
else
    $P_T \leftarrow P_T^c$
end if

B. Power allocation algorithm

Despite the capability of energy harvesting, the nanoDES requires the optimization of energy consumption, primarily for delivering its data. Once its energy content decreases below the predefined threshold, the time to refill the battery significantly increases. For example, the energy harvesting components, which harvest energy from the heart's normal periodic motion, takes about half an hour to replenish the nano-battery. Therefore, it is required to set the transmission power level of a nanoDES optimally, since the power level mainly determines the energy consumption for transmitting data to cover a certain distance. For nanonetworks, as described in Section III-A, the variation in distance as small as few millimeters has significant impact on SNR. We exploit the periodic alteration in distance between a nanoDES and the nano-macro interface and propose a distance-aware algorithm,

named as "Catch-the-pendulum" (CAP), which is given in Algorithm 1. The basic idea of the "Catch-the-pendulum" algorithm is to transmit data when the separated distance between a nanoDES and the nano-macro interface is minimal. The phrase "Catch-the-pendulum" signifies the situation when a pendulum R (assuming the rib cage with its motion) is oscillating and another pendulum H (assuming the heart and its motion) want to catch the pendulum R to deliver its message, Therefore, pendulum H requires less effort (here effort means energy) to catch pendulum R, when it is of nearest distance. The situation is illustrated in Fig. 8. On the other hand, the naive approach for power allocation, as given in Algorithm 2, ignores this periodic distance change.

VI. Performance evaluation

A. Simulation setup

We evaluated the performance of the CAP algorithm using Matlab-based simulation. However, all the data used in the simulation are experimental, which were collected from the existing literature. However, such data were manipulated according to the requirements of the algorithm and simulation scenarios. The major steps of the simulation are as follows. First, nanoDESs are assumed to be distributed randomly at certain number of clinically relevant coronary segments[2] involving LAD, RCA and LCX. The models of periodic stretching and shortening[3] of the heart muscles are added to each nanoDES, since the coronary artery is attached with the heart muscle. Next, the nano-macro interface is considered to be inserted into a certain intercostal space[4]—the position is varied according to the following rules: (1) majority nearest distance, and (2) fixed location. We applied periodic motion of the thoracic cage[5] to NM in order to compute the periodic change in distance. Meanwhile, we consider two data transmission models: (1) constant bit rate (CBR) with varying degree, and (2) Poisson data traffic, although we present results for the latter. Finally, distance between a nanoDES and the nano-macro interface is computed, and accordingly, the CAP algorithm is invoked. We executed each simulation for twenty-four hours equivalent simulation time.

In the simulations, the nanoDESs are considered to have initial energy content of 800 pJ. They harvest energy from the periodic motion of the heart, taken as 68 beat per minute. We consider the power of transmitting pulse to be in μW [29], and minimum detectable signal as 10 DB. The size of packets is chosen as 250 bytes. All the simulation parameters are listed in the Table VI-A. The topology considered in the simulation was generated randomly and it comprises of varying number of nanoDESs, as shown in Table V-B.

B. Packet delivery ratio

First, we evaluate the performance of the CAP algorithm in terms of packet delivery ratio, by varying the topology. In CAP, the ratio was higher when compared with the naive approach, as shown in Fig. 9. Note that some code IDs have packet delivery ratio close to 100% for both the approaches. Code ID refers to a nanoDES of a certain topology deployed over particular coronary segments—the mapping between a nodeID and corresponding deployed segments is given in Table V-B. This characteristic attributes to the fact that significantly less energy is consumed due to the short distance and the small variation in the change of distance, as compared with the magnitude of the harvested energy. On the other hand, differences in packet delivery ratio between CAP and the counterpart decrease when the number of nanoDES and/or data rates increases, as evident from the Topology 2. Interestingly, the nanoDES placed inside the left circumflex coronary has less packet delivery ratio, as compared to those placed inside other coronary arteries. Those nanoDESs are positioned at relatively long distances from the NM.

TABLE III
Simulation parameters

Parameter	Value
Energy per pulse	1 femtoJoule
Packet size	250 B
Heart rate	68 per min
Rib-cage rate	18 per min
Energy of nano-battery	800 picoJoule
Minimum detectable strength	10 DB
Pulse width	100 femtosecond

C. Shutdown phase

After the evaluation of packet delivery ratio, we observed that for certain nanoDESs, the amount of energy consumption for transmissions are higher than the amount of harvested energy, causing the nanoDESs to be inactive for certain periods of time, which is termed as shutdown phase. Fig. 10 depicts the shutdown phases of certain nanoDESs, which vary as much as 90%. Such high extent of shutdown indicates substantial energy consumption by the nanoDESs for transmitting data to a relatively long distant NM. Meanwhile, by adopting the CAP algorithm, some nanoDESs have no shutdown phases when compared with naive algorithm. However, higher data rates preclude such non-appearances of shutdown phases, as evident from Fig. 10(c).

D. Delay analysis

We evaluate the performance of the CAP algorithm in terms of delay, which is measured as the total time spent by transmitting 100 packets. The cap algorithm takes less time than that of its counterpart and in some cases, it takes almost 50% less time, as shown in Fig. 11. However, after transmitting few hundred packets, both the algorithms exhibit identical and small amount of delay. Afterwards, CAP spends distinct and relatively less time with certain variation, when compared with the distance-unaware approach, as evident in Fig 11. Such sudden jump on delay and then converging it to a certain value refer to the events – depletion of energy of the battery, and comparable amount of harvested energy and energy consumption for communication, respectively. It may be noted that delays of some nanoDESs of the topologies were suppressed in the figures, since such devices have identical delay due to the absence of a shutdown point.

[2]Major coronary segments can be found in [45].

[3]Such periodic deformations, reported w.r.t heart axes system [39], are computed w.r.t. the patient's body axes system, given in Appendix.

[4]Intercostal spaces are computed based on the work [46].

[5]Values of such movement can be found in [43].

TABLE I
NANODES'S CODE IDS AND THEIR MAPPING TO ANATOMICAL SEGMENTS★ OF CORONARY ARTERIES

Code ID	LAD1	LAD2	LAD3	LAD4	LAD5	LAD6	LAD7	LAD8	LAD9	LAD10	LAD11
Segments	LM mid	L1 proximal	L1 mid	L2 mid	L3 mid	L4 proximal	L4 mid	D1 origin	D1 mid	D2 origin	D2 mid
Code ID	LAD12	LAD13	LAD14	LAD15	LAD16	LAD17	LAD18	LAD19	LCX1	LCX2	LCX3
Segments	D2 mid	D3 mid	S1 origin	S1 mid	S2 origin	S2 mid	S3 origin	S3 mid	C1 proximal	C1 mid	C2 mid
Code ID	LCX4	LCX5	LCX6	LCX7	LCX8	LCX9	LCX10	LCX11	LCX12	LCX13	LCX14
Segments	C3 mid	C4 mid	MR origin	MR mid	OM origin	OM bifurcat	OM ant mid	OM pos mid	M1 origin	M1 mid	M2 origin
Code ID	LCX15	LCX16	LCX17	RCA1	RCA2	RCA3	RCA4	RCA5	RCA6	RCA7	RCA8
Segments	M2 mid	M3 origin	M3 mid	R1 proximal	R1 mid	R2 mid	R3 mid	R4 mid	RD mid	RI mid	RP mid

LAD, LCX, RCA: left, left circumflex, and right coronary artery, respectively;★segmental code is adopted from [45]

TABLE II
TOPOLOGY DESCRIPTION

Topology	**Num. of nanoDES**	**Location of nanoDES**											
		1	2	3	4	5	6	7	8	9	10	11	12
1	7	D1 MID	L1 proximal	LM mid	MR mid	RI mid	L4 MID	OM origin					
2	12	OM pos mid	D1 origin	RD mid	C1 proximal	R2 mid	M1 mid	D2 mid	S3 origin	L4 proximal	MR origin	OM birfurcat	D1 mid
3	12	L1 mid	L1 proximal	RI mid	S2 mid	M3 origin	OM ant mid	R3 mid	R1 proximal	Om pos mid	D3 mid	C4 mid	M1 mid

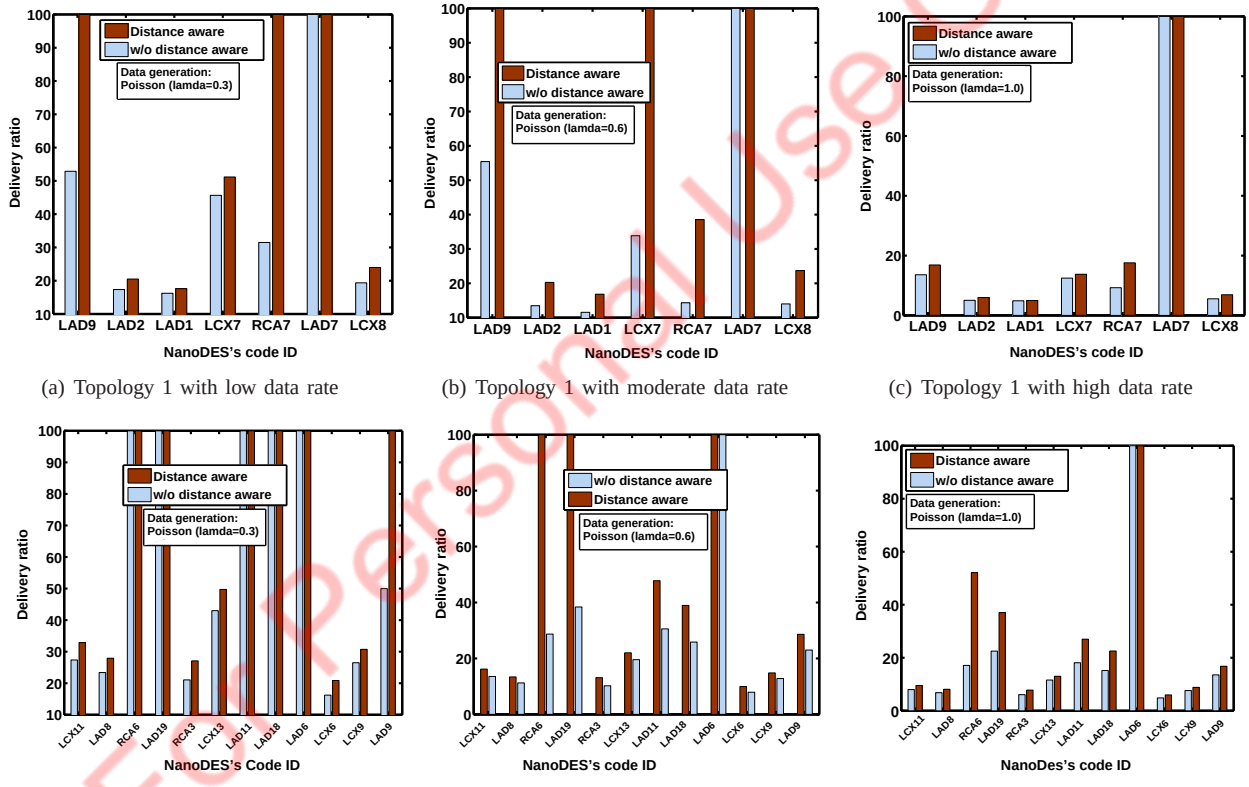

(a) Topology 1 with low data rate (b) Topology 1 with moderate data rate (c) Topology 1 with high data rate

(d) Topology 2 with low data rate (e) Topology 2 with moderate data rate (f) Topology 2 with high data rate

Fig. 9. Packet delivery ratio in different topology with multiple data rates.

E. Energy Utilization

As we observed in Section VI-B and VI-D prolongation of shutdown phase has adverse affects on packet delivery and delay, the utilization of energy between successive shutdown points provides insightful information regarding optimized energy consumption by an efficient candidate solution. For we defined the energy utilization coefficient (EUC) as follows:

$$EUC = \frac{Packet^{hit}}{Packet^{total}} \tag{10}$$

where $Packet^{hit}$ is the total number of packets that reach the NM during the period the nanoDES generates $Packet^{total}$, and transmits these assuming it to have enough energy. Fig. 12 shows the energy utlization of few[6] nanoDESs of the topology, which is used earlier for evaluating the other metrics. It may be noted that the higher the value of the coefficient, the better the energy consumption – i.e., more packets reach NM due to less energy consumption for transmission. However, some

[6]Due to space constraint, we refrain showing it for all nanoDESs, even though those using CAP have better energy utilization.

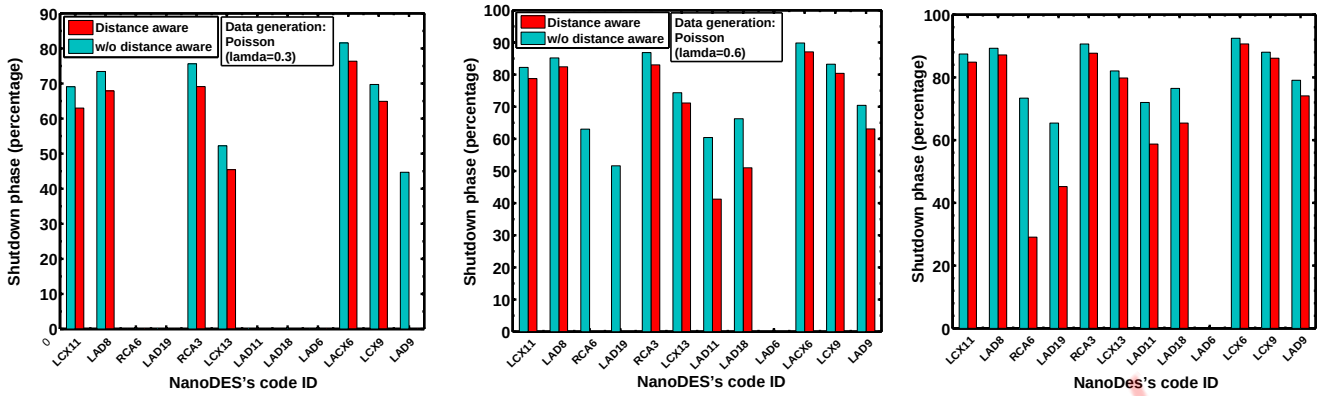

(a) (b) (c)

Fig. 10. Shutdown phase of the nanDESs of topology 2

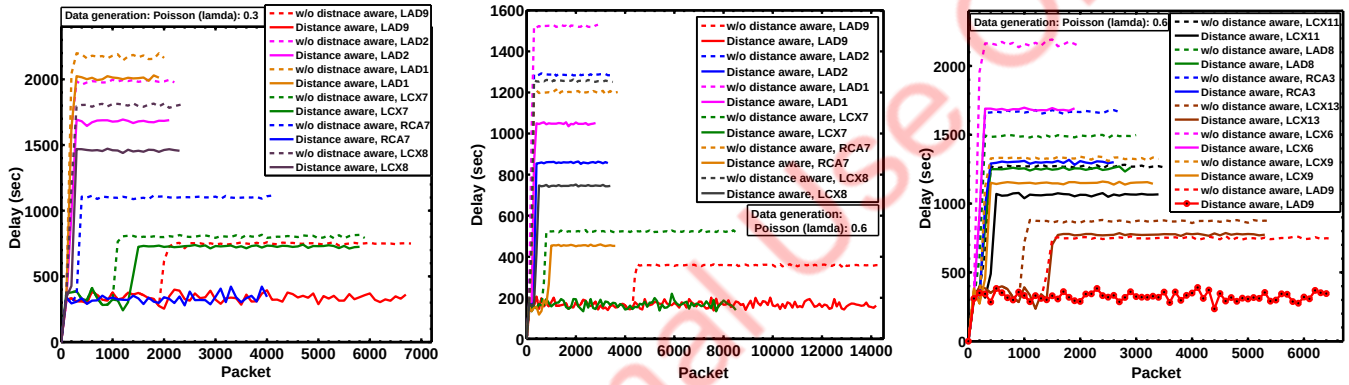

(a) Toplogy 1 and low data rate (b) Topology 1 and moderate data rate (c) Topology 2 and low data rate

Fig. 11. Delay for transmitting 100 packets taken as single unit.

nanoDES employing CAP was shown with zero EUC; this behavior indicates absence of any shutdown point. Besides, we observed that as data rate increases, CAP still outperforms the counterpart, however with less difference.

VII. Discussions and Open Challenges

A. Feasibility study of nanoDES-based CHD monitoring

To assess the feasibility of our proposed system, we first like to highlight recent advances in smart pervasive heath monitoring system *in* vivo, particularly using implantable Medical devices (IMDs). Sheppard et al. [47] described the methods of various issues – such as the placement of implantable devices, sensing biological information, actuating certain functional components, and transmitting data – for a general MEMS-based IMD. Similarly, Herman and omtov [48] and Kieval [49] depicted drug MEMS-based cardiac monitoring systems for drug delivery in in-built or programmable fashion. Furthermore, research endeavor has also been put in developing miniaturized therapeutic devices for other vital human organ monitoring and/or controlled drug delivery therein, such as programmable drug administering to eye [50], stimulating spinal cord with feedback [51], and monitoring glucose level in the blood [52].

Specifically, for combating against restenosis around stents, implantable micro-chip-embedded stents has been proposed, which have the capability of releasing therapeutic, diagnostic, and anti-restenosis agents from the integrated drug reservoirs, by either passive or active mechanism [53], [54]. Moreover, Assel et al. [55] designed sophisticated stents equipped with pressure sensors, which can read out the blood flow inside the vessel apart from monitoring the episodes of restenosis. However, continuous chronic disease monitoring with capability of delivering regular and multiple drugs often requires bigger space for the drug reservoir, and thereby precludes micro-chip to be embedded into the DESs [56]. In contrast, unprecedented advancement on Nano-Electro-Mechanical Systems (NEMS) technology has provided us tools for fabricating and packaging novel nanomaterial-based nano-scale devices, which are expected to fit well into the DESs and ultimately, inside the coronary arteries [16]. Since NEMS-based devices are relatively small, the nanoDESs are expected to incorporate more functional and communication elements, which would lead CHD monitoring system to be more precise and effective, and more convenient to end users. This improved benefit will be achieved by enabling interactive feedback and control between nano-world and macro-world communication paradigm.

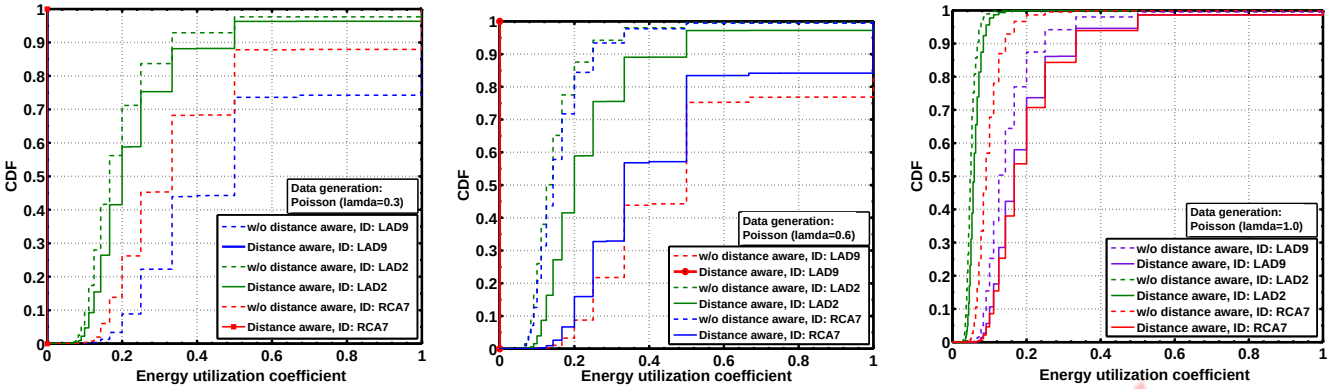

(a) Low data rate (b) Moderate data rate (c) High data rate

Fig. 12. Energy utilization between successive shutdown points of three nanoDESs of topology 1 consisting of seven nodes.

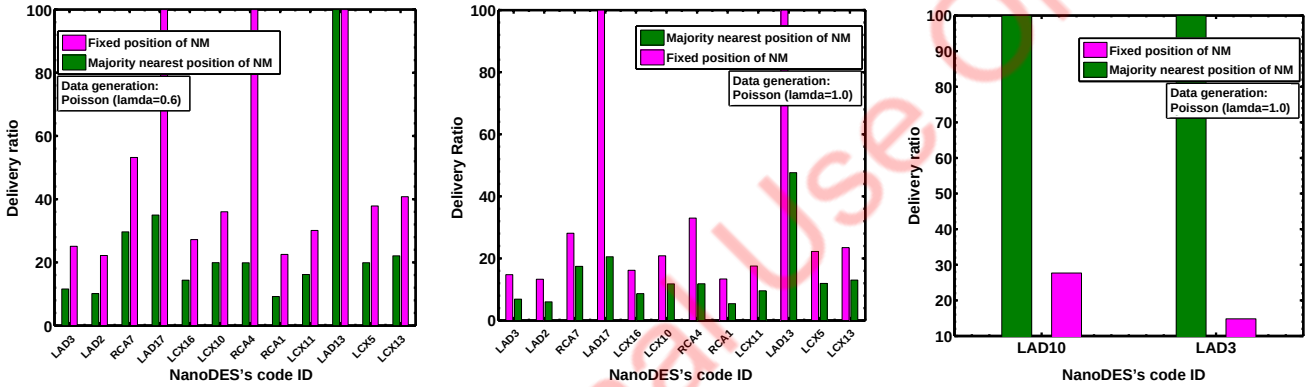

(a) Topology 3 and moderate data rate (b) Topology 3 and high data rate (c) Topology of two nanODES, generated randomly

Fig. 13. Packet delivery ratio regarding two spatial distribution of nano-macro interface

B. Placement of nano-macro interface

While evaluating the performance of the CAP algorithm, we observed that the position of the nano-macro interface inside the muscles of the ribcage plays important role, since the longer is the distance between NM and a nanoDES, the higher degradation of network performance. Intuitively, we expected that the position of the NM should be as nearest as possible to all nanoDESs, provided insertion of the interface at the particular intercostal space of the ribcage is clinically viable. Therefore, we consider the position of a NM based on two strategies: (1) majority nearest distance and (2) fixed location.

The majority nearest distance based placement works according the principle of *majority* rule—more than half of the nanoDESs of a particular topology have NM at their nearest distances. In such a strategy, all major intercostal spaces starting from second to seventh are considered in the simulation. On the other hand, fixed location, in this work, refers to the *bare area of pericardium*—the area encircled by left portion of sternocostal projection of the pericardium, which is not covered by *parietal pleura* or lungs, is used as convenient site for surgical incision.

As depicted in Fig. 13, the results shows that the packet delivery ratio of the CAP algorithm using NM at *fixed* location outweigh the strategy using *majority nearest distance*. However, a random topology of two nanoDESs perform better, following the strategy majority nearest distance, as shown in Fig. 13(c).

VIII. Conclusions and Future Work

In this paper, we envisaged nanonetworks-based CHD monitoring system and study the problem of asysmetric data delivery, which appears when transmitting data from the underlying nanoscale communication networks to macro-scale communication networks. Then, we showed that due to the channel properties of Terahertz band and limited amount of harvested energy and energy content of the nanoDESs, the reduced communication range up to few centimeters triggered this asymmetry. To circumvent such asymmetry on data delivery mechanism, we proposed a distance-aware power allocation algorithm, which exploits periodic decreases in the average distances between a nanoDES and the nano-macro interface, which are placed inside a coronary artery and intercostal space, repectively. Simulation results established robustness and efficiency of the distance-aware CAP algorithm in terms of packet delivery, energy consumption, and delay. In another experiment, we substantiated the location of NM at bare area of pericardium produced better performance as compared with

the location of NM at majority nearest distance. By enabling such mechanisms, this CHD monitoring system is expected to boast future healthcare questing towards more preemptive, preventive, and personalized healthcare.

In future, to model the deformation of heart wall more reliably, we will exhort in the model other heart wall deforming factors, such as segmental and area strain, translational and tethering, and specific deformations due to diseases including dilated cardiomyopathy, hypertropy, and hypertension as well. Similarly, to model the movement of thoracic cage, we will also include other deformations incurred by specific diseases, such as idiopathic scoliosis, and kyphoscoliosis. We also plan to validate our results with variedly demographic and ethnic datasets.

Acknowledgment

The work of the first author was supported by Maulana Azad National Fellowship, India. We express our sincere gratitude to Bikas K Arya, a Phd scholar of SMST at IIT Kharagpur, for providing some important papers.

References

[1] World Health Organization, *Global health risks: mortality and burden of disease attributable to selected major risks*. World Health Organization, 2009.

[2] C. Deaton, E. S. Froelicher, L. H. Wu, C. Ho, K. Shishani, and T. Jaarsma, "The global burden of cardiovascular disease," *European Journal of Cardiovascular Nursing*, vol. 10, no. 2 suppl, pp. S5–S13, 2011.

[3] B. Godin, J. H. Sakamoto, R. E. Serda, A. Grattoni, A. Bouamrani, and M. Ferrari, "Emerging applications of nanomedicine for the diagnosis and treatment of cardiovascular diseases," *Trends in pharmacological sciences*, vol. 31, no. 5, pp. 199–205, 2010.

[4] F. W. Mohr, M.-C. Morice, A. P. Kappetein, T. E. Feldman, E. Ståhle, A. Colombo, M. J. Mack, D. R. Holmes Jr, M.-a. Morel, N. V. Dyck, *et al.*, "Coronary artery bypass graft surgery versus percutaneous coronary intervention in patients with three-vessel disease and left main coronary disease: 5-year follow-up of the randomised, clinical syntax trial," *The Lancet*, vol. 381, no. 9867, pp. 629–638, 2013.

[5] G. Dangas and V. Fuster, "Management of restenosis after coronary intervention," *American Heart Journal*, vol. 132, no. 2, pp. 428–436, 1996.

[6] D. J. Cohen, B. Van Hout, P. W. Serruys, F. W. Mohr, C. Macaya, P. Den Heijer, M. Vrakking, K. Wang, E. M. Mahoney, S. Audi, *et al.*, "Quality of life after pci with drug-eluting stents or coronary-artery bypass surgery," *New England Journal of Medicine*, vol. 364, no. 11, pp. 1016–1026, 2011.

[7] J. W. Jukema, J. J. Verschuren, T. A. Ahmed, and P. H. Quax, "Restenosis after pci. part 1: pathophysiology and risk factors," *Nature Reviews Cardiology*, vol. 9, no. 1, pp. 53–62, 2011.

[8] G. W. Stone, A. Maehara, A. J. Lansky, B. de Bruyne, E. Cristea, G. S. Mintz, R. Mehran, J. McPherson, N. Farhat, S. P. Marso, *et al.*, "A prospective natural-history study of coronary atherosclerosis," *New England Journal of Medicine*, vol. 364, no. 3, pp. 226–235, 2011.

[9] T. I. Chang, T. K. Leong, D. S. Kazi, H. S. Lee, M. A. Hlatky, and A. S. Go, "Comparative effectiveness of coronary artery bypass grafting and percutaneous coronary intervention for multivessel coronary disease in a community-based population with chronic kidney disease," *American Heart Journal*, vol. 165, no. 5, pp. 800–808, 2013.

[10] M. E. Farkouh, M. Domanski, L. A. Sleeper, F. S. Siami, G. Dangas, M. Mack, M. Yang, D. J. Cohen, Y. Rosenberg, S. D. Solomon, *et al.*, "Strategies for multivessel revascularization in patients with diabetes," *New England Journal of Medicine*, vol. 367, no. 25, pp. 2375–2384, 2012.

[11] C. Kaiser, S. Galatius, P. Erne, F. Eberli, H. Alber, H. Rickli, G. Pedrazzini, B. Hornig, O. Bertel, P. Bonetti, *et al.*, "Drug-eluting versus bare-metal stents in large coronary arteries," *New England Journal of Medicine*, vol. 363, no. 24, pp. 2310–2319, 2010.

[12] S. Venkatraman and F. Boey, "Release profiles in drug-eluting stents: issues and uncertainties," *Journal of controlled release*, vol. 120, no. 3, pp. 149–160, 2007.

[13] J. Hausleiter, A. Kastrati, R. Wessely, A. Dibra, J. Mehilli, T. Schratzenstaller, I. Graf, M. Renke-Gluszko, B. Behnisch, J. Dirschinger, *et al.*, "Prevention of restenosis by a novel drug-eluting stent system with a dose-adjustable, polymer-free, on-site stent coating," *European heart Journal*, vol. 26, no. 15, pp. 1475–1481, 2005.

[14] A. J. Carter, M. Aggarwal, G. A. Kopia, F. Tio, P. S. Tsao, R. Kolata, A. C. Yeung, G. Llanos, J. Dooley, and R. Falotico, "Long-term effects of polymer-based, slow-release, sirolimus-eluting stents in a porcine coronary model," *Cardiovascular research*, vol. 63, no. 4, pp. 617–624, 2004.

[15] I. F. Akyildiz, J. M. Jornet, and M. Pierobon, "Nanonetworks: A new frontier in communications," *Communications of the ACM*, vol. 54, no. 11, pp. 84–89, 2011.

[16] R.-X. Yin, D.-Z. Yang, and J.-Z. Wu, "Nanoparticle drug-and gene-eluting stents for the prevention and treatment of coronary restenosis," *Theranostics*, vol. 4, no. 2, p. 175, 2014.

[17] D. Malak and O. B. Akan, "Molecular communication nanonetworks inside human body," *Nano Communication Networks*, vol. 3, no. 1, pp. 19–35, 2012.

[18] H. Guo, P. Johari, J. Jornet, and Z. Sun, "Intra-body optical channel modeling for in-vivo wireless nanosensor networks," *IEEE transactions on NanoBioscience*, 2015. doi:10.1109/TNB.2015.2508042.

[19] G. Piro, K. Yang, G. Boggia, N. Chopra, L. A. Grieco, and A. Alomainy, "Terahertz communications in human tissues at the nanoscale for healthcare applications," *IEEE Transactions on Nanotechnology*, vol. 14, no. 3, pp. 404–406, 2015.

[20] S. Misra, N. Islam, J. Mahapatro, and J. J. Rodrigues, "Green wireless body area nanonetworks: Energy management and the game of survival," *IEEE Journal of Biomedical and Health Informatics*, vol. 18, no. 2, pp. 467–475, 2014.

[21] J. A. Stankovic, "Research directions for the internet of things," *IEEE Journal on Internet of Things*, vol. 1, no. 1, pp. 3–9, 2014.

[22] I. Akyildiz, M. Pierobon, S. Balasubramaniam, and Y. Koucheryavy, "The internet of bio-nano things," *IEEE Communications Magazine*, vol. 53, no. 3, pp. 32–40, 2015.

[23] K. Han, J. Luo, Y. Liu, and A. V. Vasilakos, "Algorithm design for data communications in duty-cycled wireless sensor networks: A survey," *IEEE Communications Magazine*, vol. 51, no. 7, pp. 107–113, 2013.

[24] D. S. De Couto, D. Aguayo, J. Bicket, and R. Morris, "A high-throughput path metric for multi-hop wireless routing," *Wireless Networks*, vol. 11, no. 4, pp. 419–434, 2005.

[25] G. Lu, N. Sadagopan, B. Krishnamachari, and A. Goel, "Delay efficient sleep scheduling in wireless sensor networks," in *Proceedings of IEEE 24th Annual Joint Conference of the IEEE Computer and Communications Societies, INFOCOM 2005*, vol. 4, pp. 2470–2481, IEEE, 2005.

[26] Y. Gu and T. He, "Dynamic switching-based data forwarding for low-duty-cycle wireless sensor networks," *Mobile Computing, IEEE Transactions on*, vol. 10, no. 12, pp. 1741–1754, 2011.

[27] W. Zhao, M. Ammar, and E. Zegura, "A message ferrying approach for data delivery in sparse mobile ad hoc networks," in *Proceedings of the 5th ACM international symposium on Mobile ad hoc networking and computing*, pp. 187–198, ACM, 2004.

[28] A. Lindgren, A. Doria, and O. Schelen, "Probabilistic routing in intermittently connected networks," in *Service assurance with partial and intermittent resources*, pp. 239–254, Springer, 2004.

[29] J. M. Jornet and I. F. Akyildiz, "Femtosecond-long pulse-based modulation for terahertz band communication in nanonetworks," *IEEE Transactions on Communications*, vol. 62, no. 5, pp. 1742–1754, 2014.

[30] P. Boronin, V. Petrov, D. Moltchanov, Y. Koucheryavy, and J. M. Jornet, "Capacity and throughput analysis of nanoscale machine communication through transparency windows in the terahertz band," *Nano Communication Networks*, vol. 5, no. 3, pp. 72–82, 2014.

[31] R. Piesiewicz, T. Kleine-Ostmann, N. Krumbholz, D. Mittleman, M. Koch, J. Schoebel, and T. Kurner, "Short-range ultra-broadband terahertz communications: Concepts and perspectives," *IEEE Antennas and Propagation Magazine*, vol. 49, no. 6, pp. 24–39, 2007.

[32] R. Piesiewicz, M. Jacob, M. Koch, J. Schoebel, and T. Kurner, "Performance analysis of future multigigabit wireless communication systems at thz frequencies with highly directive antennas in realistic indoor environments," *IEEE Journal of Selected Topics in Quantum Electronics*, vol. 14, no. 2, pp. 421–430, 2008.

[33] K. Yang, A. Alomainy, and Y. Hao, "In-vivo characterisation and numerical analysis of the thz radio channel for nanoscale body-centric wireless networks," in *Radio Science Meeting (Joint with AP-S Symposium), 2013 USNC-URSI*, pp. 218–219, IEEE, 2013.

[34] IEEE Standards Coordinating Committee 28 on Non-Ionizing Radiation Hazards, *IEEE Standard for Safety Levels with Respect to Human*

Exposure to Radio Frequency Electromagnetic Fields, 3kHz to 300 GHz. Institute of Electrical and Electonics Engineers, Incorporated, 1992.

[35] S. Gabriel, R. Lau, and C. Gabriel, "The dielectric properties of biological tissues: Ii. measurements in the frequency range 10 hz to 20 ghz," *Physics in medicine and biology*, vol. 41, no. 11, p. 2251, 1996.

[36] R. Bashirullah, "Wireless implants," *IEEE Microwave Magazine*, vol. 11, no. 7, pp. S14–S23, 2010.

[37] J. M. Jornet and I. F. Akyildiz, "Joint energy harvesting and communication analysis for perpetual wireless nanosensor networks in the terahertz band," *IEEE Transactions on Nanotechnology*, vol. 11, no. 3, pp. 570–580, 2012.

[38] S. E. Smith and G. E. Darling, "Surface anatomy and surface landmarks for thoracic surgery: Part ii," *Thoracic surgery clinics*, vol. 21, no. 2, pp. 139–155, 2011.

[39] J. Dumesnil, R. Shoucri, J. Laurenceau, and J. Turcot, "A mathematical model of the dynamic geometry of the intact left ventricle and its application to clinical data.," *Circulation*, vol. 59, no. 5, pp. 1024–1034, 1979.

[40] "Strain rate imaging." http://folk.ntnu.no/stoylen/strainrate, 2009. [online; Accessed on January 15, 2016].

[41] J.-U. Voigt, G. Pedrizzetti, P. Lysyansky, T. H. Marwick, H. Houle, R. Baumann, S. Pedri, Y. Ito, Y. Abe, S. Metz, *et al.*, "Definitions for a common standard for 2d speckle tracking echocardiography: consensus document of the eacvi/ase/industry task force to standardize deformation imaging," *European Heart Journal of Cardiovascular Imaging*, p. jeu184, 2014.

[42] J. Leong, W. Lu, K. Luk, and E. Karlberg, "Kinematics of the chest cage and spine during breathing in healthy individuals and in patients with adolescent idiopathic scoliosis," *Spine*, vol. 24, no. 13, p. 1310, 1999.

[43] J. Jordanoglou, "Rib movement in health, kyphoscoliosis, and ankylosing spondylitis," *Thorax*, vol. 24, no. 4, pp. 407–414, 1969.

[44] R. M. Lang, L. P. Badano, V. Mor-Avi, J. Afilalo, A. Armstrong, L. Ernande, F. A. Flachskampf, E. Foster, S. A. Goldstein, T. Kuznetsova, *et al.*, "Recommendations for cardiac chamber quantification by echocardiography in adults: an update from the american society of echocardiography and the european association of cardiovascular imaging," *Journal of the American Society of Echocardiography*, vol. 28, no. 1, pp. 1–39, 2015.

[45] J. Dodge, B. G. Brown, E. L. Bolson, and H. T. Dodge, "Intrathoracic spatial location of specified coronary segments on the normal human heart. applications in quantitative arteriography, assessment of regional risk and contraction, and anatomic display.," *Circulation*, vol. 78, no. 5, pp. 1167–1180, 1988.

[46] L. K. Fujimoto, G. Jacobs, J. Przybysz, S. Collins, T. Meaney, W. A. Smith, R. J. Kiraly, and Y. Nosé, "Human thoracic anatomy based on computed tomography for development of a totally implantable left ventricular assist system," *Artificial organs*, vol. 8, no. 4, pp. 436–444, 1984.

[47] N. F. Sheppard Jr, J. T. Santini Jr, M. J. Cima, R. S. Langer, and D. Ausiello, "Method for wirelessly monitoring implanted medical device," Mar. 26 2013. US Patent 8,403,907.

[48] S. J. Herman and B. M. Yomtov, "Medical device for controlled drug delivery and cardiac monitoring and/or stimulation," Mar. 29 2011. US Patent 7,917,208.

[49] R. S. Kieval, "Drug delivery neural stimulation device for treatment of cardiovascular disorders," Jan. 23 2001. US Patent 6,178,349.

[50] J. T. Santini Jr, M. J. Cima, R. S. Langer, D. Ausiello, N. F. Sheppard Jr, and S. J. Herman, "Method and system for drug delivery to the eye," Nov. 13 2012. US Patent 8,308,707.

[51] W. Grill and T. ZHANG, "Systems and methods for administering spinal cord stimulation based on temporal patterns of electrical stimulation." https://www.google.com/patents/WO2014159880A1?cl=en, Oct. 2 2014. WO Patent App. PCT/US2014/025,389.

[52] S. K. Vashist, "Continuous glucose monitoring systems: A review," *Diagnostics*, vol. 3, no. 4, pp. 385–412, 2013.

[53] E. Meng and T. Hoang, "Micro-and nano-fabricated implantable drug-delivery systems," *Therapeutic delivery*, vol. 3, no. 12, pp. 1457–1467, 2012.

[54] J. T. Santini Jr and C. E. Hutchinson, "Implantable drug delivery stents," Dec. 2 2003. US Patent 6,656,162.

[55] T. Assel, C. Cuddalore, W. D. Leon-Salas, and C. H. Lee, "Smart cardiovascular stent against in-stent restenosis," *Abstracts (Missouri Regional Life Sciences Summit 2010)*, 2010.

[56] M. Staples, K. Daniel, M. J. Cima, and R. Langer, "Application of micro- and nano-electromechanical devices to drug delivery," *Pharmaceutical research*, vol. 23, no. 5, pp. 847–863, 2006.

APPENDIX A
DERIVATION OF AMPLITUDES FOR THREE DIRECTIONAL SHORTENING W.R.T. PATIENT COORDINATE SYSTEM

A. Longitudinal Shortening

Longitudinal shortening is due to the periodic deformation of longitudinal fibre muscles along the long axis of heart (as shown in Fig. 3). Since the magnitudes of such deformations are typically reported with respect to the heart axes system (which is considered as local coordinate system in this paper), the required transformations with respect to the patient's body coordinates system are computed as follows. The first transformation breaks the longitudinal deformation along axis of the heart into two orthogonal dimensions: $L_{z'} = L\cos\alpha$, and$L_{xy} = L\sin\alpha$, where L and α refer to magnitudes of longitudinal shortening and angle between the long axes of body and heart, respectively. Note that magnitude of the angle varies depending on anatomical orientation of an individual's cardiac axis, and in most cases it lies around $45°$, which is considered in this paper for simulation. Further, the second transformation, applied on the two orthogonal components, produces vectors regarding patient's body axes system, which are given as follows:

$$\begin{aligned} L_z &= L_{z'}\cos\beta = L\cos\alpha\cos\beta \quad \text{in AP direction, and} \\ L_{Y_1} &= L_{z'}\sin\beta = L\cos\alpha\sin\beta \quad \text{in vertical direction} \end{aligned} \tag{11}$$

and

$$\begin{aligned} L_x &= L_{xy}\cos\beta = L\sin\alpha\cos\beta \quad \text{in lateral direction, and} \\ L_{Y_2} &= L_{xy}\sin\beta = L\sin\alpha\sin\beta \quad \text{in vertical direction.} \end{aligned} \tag{12}$$

where β is the angle between transverse plane, containing AP and lateral axes, and the direction of long axis of heart. After combining (11) and (12), finally the three components of the longitudinal shortening, with respect to body axes system – i.e., lateral, vertical, and AP directions, repectively – is computed as follows:

$$\begin{aligned} L_x &= L\sin\alpha\cos\beta; \\ L_y &= L_{Y_1} + L_{Y_1} = L\sin\beta(\cos\alpha + \sin\alpha); \\ L_z &= L\cos\alpha\cos\beta. \end{aligned} \tag{13}$$

B. Circumferential shortening

This type of shortening refers to shortening of the defined circumference, and as circumference measured in terms of diameter, the change of the diameter reflects measurement of shortening of the designated circumference. For this work, radius of the circumference is chosen as the mid-wall (the wall consisting of endocardium and pericardium as opposite boundaries, as shown in Fig. 7) radius. If R is the magnitude of the circumferential shortening of the midwall with respect to the local heart axes system, the components along the vertical direction, and its normal plane corresponding to patient's body axes system can be written as follows:

$$\begin{aligned} R_y &= R\cos\beta \text{ and} \\ R_{zx} &= R\sin\beta \end{aligned} \tag{14}$$

Further, R_{zx} is divided in two orthogonal components, which are given below:

$$R_x = R_{zx} \sin\beta \sin\gamma \text{ in lateral direction and,} \quad (15)$$
$$R_z = R_{zx} \sin\beta \cos\gamma \text{ in AP direction,} \quad (16)$$

where γ is the angle between the plane containing AP and vertical axes, and the plane containing the the vector R_{zx}.

C. Wall thickening

Let T be the value of the wall thickness at the peak of systolic event and measured with respect to heart axes system. In patient body axes system, the value of thickness can be written as:

$$T_y = T \cos\beta \text{ in vertical direction and} \quad (17)$$
$$T_{zx} = T \sin\beta$$

Similarly, T_{zx} can be represented in two orthogonal components, which are given as follows:

$$T_x = T_{zx} \sin\beta \sin\gamma \text{ in lateral direction and,} \quad (18)$$
$$T_z = T_{zx} \sin\beta \cos\gamma \text{ in AP direction.} \quad (19)$$

The aggregation of all three shortening results in the left ventricle to contract radially and longitudinally. Combining Equations (11), (12), (13), (14), (15), (17), (18), and (19), such radial and longitudinal shortening regarding heart axes system can be expressed in the required three dimensional patient body axes system, which are given below:

$$\begin{aligned} t &= -L_x - R_x + T_x \\ &= (T-R)\sin\beta\sin\gamma - L\sin\alpha\cos\beta \text{ in lateral direction;} \end{aligned} \quad (20)$$

$$\begin{aligned} r &= -L_y - R_y + T_y \\ &= (T-R)\cos\beta - L\sin\beta(\sin\alpha + \cos\alpha) \text{ in vertical direction;} \end{aligned} \quad (21)$$

$$\begin{aligned} l &= -L_z - R_z + T_z \\ &= (T-R)\sin\beta\cos\gamma - L\cos\alpha\cos\beta \text{ in AP direction.} \end{aligned} \quad (22)$$

Note that the negative sign indicates the actual shortening, whereas positive sign refers to the wall thickening during systolic event.